Chandra X-Ray Observations of the Young Open Cluster NGC 2516

F. Damiani, E. Flaccomio, G. Micela, S. Sciortino

INAF - Osservatorio Astronomico di Palermo G.S.Vaiana, Piazza del Parlamento 1, I-90134 Palermo, ITALY

damiani@oapa.astropa.unipa.it, ettoref@oapa.astropa.unipa.it, giusi@oapa.astropa.unipa.it, sciorti@oapa.astropa.unipa.it

and

F. R. Harnden Jr., S. S. Murray, S. J. Wolk

Smithsonian Astrophysical Observatory, 60 Garden Street, Cambridge, MA 02138

frh@cfa.harvard.edu, ssm@cfa.harvard.edu, swolk@cfa.harvard.edu

and

R. D. Jeffries

Department of Physics, Keele University, Keele, Staffordshire ST5 5BG, United Kingdom

rdj@astro.keele.ac.uk

ABSTRACT

We present a comprehensive study of the Chandra X-ray observations of the young open cluster NGC 2516. We have analyzed 8 individual Chandra observations. We have combined the data to achieve the greatest sensitivity, reaching down to $\log f_X = -14.56$ (ergs/sec/cm^{-2}), or $\log L_X = 28.69$ (ergs/sec) at the distance of NGC 2516. Out of 284 X-ray sources detected, 155 are identified with photometric cluster members, with very little ambiguity. We have studied the X-ray luminosity functions for the various spectral types, correcting for non-member contamination those for later type stars. We find strong X-ray emission from a couple B stars, that cannot be due to companions. Among A stars, chemically peculiar stars show a detection fraction much larger than normal A stars. The luminosity functions decrease monotonically from F to M stars, and those for K stars are significantly lower than similar stars in the Pleiades, a cluster only slightly younger than NGC 2516. We discuss possible causes of this discrepancy, including differences in age and stellar rotation.

Subject headings: open clusters and associations: individual (NGC 2516) — stars: coronae — X-rays: stars

1. Introduction

The young southern open cluster NGC 2516 has been studied with increased interest in the last decade. It bears many similarities with the well-studied Pleiades cluster, however it differs in some non-negligible respects. NGC 2516 is only slightly older than the Pleiades: Mermilliod (1981) estimates its age as 107 Myr, to be compared with 78 Myr of the Pleiades. Other authors (e.g. Snowden 1975) give a different age estimate, but about the same relative age with respect to the Pleiades. However, it appears to contain many more stars than the Pleiades, both of high mass (Dachs 1970), and of low mass (Jeffries et al. 2001). There are various estimates of its distance modulus, most of which in agreement with the value 7.94, or $d = 387$ pc, given by Jeffries et al. (1997), that will be adopted here. The Hipparcos data yield for NGC 2516 a distance of $d = 346.0^{+27.1}_{-23.4}$ pc (Robichon et al. 1999), in agreement within 1.5 sigmas with the Jeffries et al. value.

Unlike the Pleiades, NGC 2516 contains a few chemically peculiar Ap stars (Dachs 1970). However, spectra exist only for the brighter cluster members, while for most putative members they are still lacking. This is especially unfortunate, since in recent years doubts have arisen about the chemical composition of the cluster stars. Jeffries et al. (2001, and references therein) have found, on the basis of photometric data, a probable metal under-abundance by a factor of 2 with respect to the Sun (and to the Pleiades). Analogous results by other authors seem to lead to a consensus that this is actually the case. However, in a more recent work, Terndrup et al. (2002) find a solar-like metal abundance for NGC 2516, on the basis of high-resolution spectra.

NGC 2516 has also been studied in X-rays with ROSAT, using both the PSPC (Dachs and Hummel 1996, Jeffries et al. 1997), and the HRI (Micela et al. 2000). Based on the optical member lists available at that time, some differences were already found in the NGC 2516 X-ray luminosity functions with respect to Pleiades stars. In particular, the G and K stars in NGC 2516 were found to be underactive in X-rays with respect to the Pleiades G and K stars, while no such difference was found for M stars. Jeffries et al. (1997) thoroughly discuss how these differences could be related to a low-metallicity effect, through a different evolution of the stellar internal structure. On the light of the new high-resolution optical data, these explanations cannot hold any more. Our purpose here is to first ascertain, on the basis of the new, higher-quality X-ray data made available using Chandra if differences with respect to the Pleiades X-ray emission persist, and then to obtain clues about the origin of any peculiarity of the X-ray emission of NGC 2516. A preliminary analysis was made by Harnden et al. (2001), using a subset of the Chandra data that we study in this work. NGC 2516 was also observed with XMM-Newton, and the analysis of two observation segments was made by Sciortino et al. (2001). The analysis of additional segments is underway (Pillitteri et al. in preparation).

The larger distance of NGC 2516 with respect to the Pleiades requires that proportionally more sensitive X-ray observations are needed to study the two clusters with comparable detail. Moreover, the apparent X-ray source density is also larger in NGC 2516, that makes high spatial resolution highly desirable, especially in order to obtain unambiguous X-ray-optical identifications. As we will see in section 4, the Chandra data analyzed here are almost ideal in this respect. By comparison, the XMM-Newton data become increasingly confused near the cluster center, as the limiting sensitivity goes deeper.

2. Chandra Data on NGC 2516

NGC 2516 has been observed by Chandra with all its detectors in imaging mode, three times with the HRC-I, once with the HRC-S, twice with ACIS-I, twice with ACIS-S, and once with a non-standard ACIS chip configuration. The HRC-S observation contains little new information, and presents special difficulties for its analysis, and therefore has not been considered in this work. Therefore, we have analyzed eight individual pointings, whose details are reported in Table 1. The deep HRC-I observation ObsId 27 was part of the HRC-team GTO observation program, while all other pointings were taken as calibration datasets, to determine accurate bore-sight corrections for all imaging detectors, due to the availability of a number of moderately bright point sources over a suitable sky area.

The target coordinates of all NGC 2516 pointings (except for ObsId 1458) lie within $2'$ from one another, and from cluster center. ObsId 1458 was targeted $9.5'$ southward, but there is still a large overlap between its field of view and those of all other ObsIds.

We recall briefly some properties of the relevant Chandra instruments used in this work. HRC-I is a micro-channel plate, covering $32' \times 32'$ on the sky, with $0.127''$ pixels that adequately sample the on-axis Chandra PSF ($0.5''$ FWHM). While its intrinsic sensitivity is rather uniform, its true sensitivity is dominated by telescope vignetting and off-axis widening of the PSF. ACIS-I is a smaller ($16' \times 16'$) but more sensitive CCD-mosaic detector, made of 2×2 front-illuminated (FI) chips. ACIS-S is instead a linear array ($8' \times 48'$) of 6 CCDs, alternating front-illuminated and back-illuminated (BI) chips. Since FI and BI chips have different properties (sensitivity, background level), this poses special problems in the analysis of ACIS-S images. Moreover, all ACIS CCDs can be operated independently, and any choice of up to 6 chips is in principle possible, allowing non-standard configurations such as ObsId 1458, where chips 2,3,6,7,8 were used. The ACIS pixel size is $0.5''$, and therefore undersamples the on-axis Chandra PSF. HRC allows accurate timing of recorded X-ray events, but has no spectral resolution. On the contrary, the standard ACIS observing mode (as in our case) yields a time resolution of only about 3.2 sec, but gives moderate (R$\sim 35-50$) resolution spectral information.

The fields of view of all Chandra pointings used in this work are shown in Figure 1, overlaid on the optical DSS red image of NGC 2516.

Table 1: Observation journal for NGC 2516

ObsId	RA (J2000)	Dec (J2000)	Date	Detector	Raw T_{exp} (s)	Raw events	Screened T_{exp} (s)	Screened events
66	7:58:05.6	–60:45:19.7	1999-08-22	ACIS-S	11914.34	628199	9904.96	244768
1229	7:58:05.6	–60:45:19.7	1999-08-22	ACIS-S	10930.38	556535	10930.38	205524
65	7:58:20.1	–60:47:20.4	1999-08-26	ACIS-I	20155.78	723201	9901.81	109006
1232	7:58:20.1	–60:47:20.3	1999-08-27	ACIS-I	10685.11	1807826	8499.00	740878
1405	7:58:08.3	–60:45:21.1	1999-10-25	HRC-I	20304.46	1012792	20204.56	531202
1458	7:58:16.8	–60:54:59.2	1999-11-02	ACIS[a]	11585.49	474787	9652.21	26606
27	7:58:08.5	–60:45:50.1	2000-02-15	HRC-I	49303.32	3105919	42156.83	1243781
999	7:58:20.0	–60:46:22.4	2001-03-05	HRC-I	18088.14	837823	18076.93	451524

[a]Used a non-standard choice of chips: 2,3,6,7, and 8

3. X-Ray Data Analysis

We have first analyzed separately each of the eight NGC 2516 Chandra observations, to derive lists of detected sources with their X-ray fluxes and apparent sizes. Then, we have taken advantage of the rather unique opportunity offered by the large overlap of these observations, to achieve a deeper sensitivity by combining many pointings together, as we explain in detail in Section 3.2.

Before starting analysis, we have cleaned our data, removing known hot pixels and bad columns. To reject most non-X-ray events we have selected ACIS events with grades=0,2,3,4,6 in the energy band 0.3-8.0 keV. For HRC-I, we have selected photons in the PHA range 35-600, since outside of this range one only finds non-X-ray events. Moreover, we have developed a method to maximize the signal/noise ratio of weak sources, screening out time intervals with high background level. These occur occasionally, especially because of eruptive solar events, and on time scales typically shorter than the length of an individual Chandra observation, and they are sometimes very evident in the background lightcurve of an observation. It can be shown that rejecting all photons recorded when the background level is higher than a certain threshold, the signal/noise ratio of weak sources reaches a maximum, usually larger than if no rejection is made. We have therefore computed the background threshold relative to each of our observations, and discarded all time intervals with higher background.

In Table 1 we list for each pointing its raw exposure time and number of events (as in Level 1 processed data), and the exposure time and number of events after screening. In some cases, the amount of time rejected because of high background is substantial, and in these instances our screening permits a dramatic improvement in the signal/noise ratio of weak sources.

For each dataset, we have computed an exposure map (using the CIAO task mkexpmap), using spectral weights appropriate to a thermal MEKAL model with temperature 0.5 keV and absorption $N_H = 7.0 \times 10^{20}$ cm^{-2}, to mimic the spectrum expected for X-ray sources in our cluster. For ACIS-S, separate exposure maps were computed for FI and BI chips, respectively, since they have markedly different sensitivities.

3.1. Individual Pointings

Source detection was performed for each individual dataset using *Pwdetect*, a wavelet-transform detection algorithm recently developed at the Osservatorio Astronomico di Palermo (Damiani et al. in preparation), on the basis of its ROSAT predecessor called *wdetect* (Damiani et al. 1997a,b)[1]. Like other wavelet-based detection methods, it performs a multi-scale search for sources, that can range from pointlike up to $0.3'$ or more. The main features of *Pwdetect* are the following: 1) It works directly on (unbinned) event lists, that permits a complete exploration of the spatial information contained in Chandra observations, without the inefficiency intrinsic to huge full-resolution images, nor the spatial degradation of rebinned images. 2) It uses exposure maps to correct for underexposed regions (e.g. ACIS gaps) and to derive accurate source fluxes. 3) It computes reference maps of the background, that take into account its strictly Poisson statistics, and are accurate even in the limit of very low background (per resolution element), minimizing the effect of nearby point sources. 4) It has been extensively tested on large sets of pure-background Chandra simulations, from which were derived the appropriate thresholds to obtain a desired number of spurious detections per field.

Since the actual Chandra PSF is not gaussian, as assumed by *Pwdetect*, we needed to apply a correction factor to the detected source count rates. This factor was derived by computing the wavelet transform of the calibration PSFs at different positions across the field of view, separately for each Chandra detector. This amounted to a count-rate correction of up to 30% near the center, and more typically 10-15%, for a representative energy of 1.4967 keV. From a study of the HRC image of Orion Trapezium (Flaccomio et al. 2002), we have learned that the HRC calibration PSFs need first to be convolved with a gaussian with $\sigma = 0.3$". The same study has also shown that the maximum positional error due to PSF distortion is $0.8''$ for off-axis angles up to $10'$, and $1.5''$ across the whole field of view.

For this work, we use a modified version of *Pwdetect*, that also computes upper limits for undetected objects. We compute upper limits for all NGC 2516 candidate members from optical photometry listed by Jeffries et al. (2001) (see section 4), plus brighter members listed by Jeffries et al. (1997). The optical survey of Jeffries et al. (2001) covers completely the spatial region of our X-ray study. To these optical star positions, we have added X-ray source positions detected in at least one of our Chandra pointings of NGC 2516. The same PSF-related correction factor was applied to the upper-limit count rates computed by *Pwdetect*.

We have chosen for each pointing a threshold corresponding to one spurious detection per field. Since the integrated background varies from one dataset to another, the threshold varies accordingly. After running *Pwdetect*, the detected source list for each dataset was

[1] *Pwdetect* is now available publically at the address:
http://www.astropa.unipa.it/progetti_ricerca/PWDetect/

carefully checked for possible "double" detections, namely X-ray sources that *Pwdetect* splits each in two detections, since it is mislead by the elongated off-axis PSF shape. The effect of this strongly non-circular PSF on the detection procedure is difficult to correct in general terms, and we have found more convenient to "clean" the *Pwdetect* source lists afterwards. Visually, these double detections are easily recognized since all detection pairs in the same neighborhood are oriented nearly in the same direction, following the PSF elongation. To do this cleaning more automatically, we have found that a good rule for our NGC 2516 fields is to merge into one source all pairs with separation $d < 2\Delta r$ (where Δr is the *Pwdetect* computed positional error) or $d < 3.5$". This latter term accounts for the PSF distortion. Only one source pair (in ObsId 1458) not satisfying these conditions appears to be real, and has been therefore retained in the final source list. All detections are pointlike sources.

In ACIS-S datasets, there are adjacent FI and BI chips, with very different background levels. These were analyzed separately with *Pwdetect*, and the resulting source lists merged. No sources were detected in ACIS-S chips 4 and 9. Chip 8 is affected by severe instrumental noise (streaks), and although this may be corrected it does not contain obvious sources in our observations. The *Pwdetect* results for all individual NGC 2516 Chandra datasets, after cleaning, are summarized in Table 2. In the Table, ACIS-I refers to chips 0123, analyzed together. When ACIS chips are analyzed individually, detections are listed in their respective columns.

Table 2: Number of detections and sensitivity for individual NGC 2516 pointings

ObsId	Number of Detections:								Total	Lowest Det.Flux
	HRC-I	ACIS-I	ACIS CCD_ID							$(cnt/s/cm^2)$
			2	3	5	6	7			
66					1	30	35		66	1.46×10^{-6}
1229					0	29	34		63	1.32×10^{-6}
65		126				3	1		130	1.81×10^{-6}
1232		72				0	1		73	2.48×10^{-6}
1405	80								80	1.57×10^{-6}
1458			5	5		35	43		88	0.96×10^{-6}
27	116								116	0.94×10^{-6}
999	74								74	2.10×10^{-6}

3.2. Summed Pointings

The three HRC-I observations ObsIds 27, 1405 and 999, and the two ACIS-I observations ObsIds 65 and 1232 are pointed within $2'$ of one another, and their fields of view are homogeneous (no FI-BI chips alternance). Therefore, we have modified our *Pwdetect* code in a way to enable it to detect sources in a combined dataset, comprising all photons of the 3 HRC-I and 2 ACIS-I datasets just mentioned. Of course, this has required also to combine the individual exposure maps of all input datasets, built as explained in the previous section.

Combining event lists (or images) pertaining to detectors with different properties is not trivial. We have chosen to combine only datasets without strong discontinuities inside them. We have also made certain that the pointing is nearly the same, so that the PSF does not change very much from one to another (the Chandra PSF is essentially constant within a radius of about $4'$ from center, and varies sufficiently slowly outside $4'$). Finally, to derive meaningful source fluxes one has to use exposure maps in "physical units", i.e. not just time but time$\times$cm^2. In this way we can combine datasets obtained with HRC-I and with ACIS-I (whose effective areas differ by about a factor of 3) and still derive reliable source fluxes.

Another matter of concern is whether residual errors in the Chandra aspect reconstruction between different observations exist, as they need to be corrected before combining datasets. We have evaluated these shifts as median offsets between matching detections in different datasets, and they turn out to be at most about $0.35''$, enough to distort significantly the on-axis PSF. We have therefore shifted each input event list accordingly (with respect to the mean position of all datasets).

Using the upgraded *Pwdetect*, we detect 189 sources in the combined (3 HRC-I + 2 ACIS-I) dataset, with only one spurious expected, with the lowest detection having a photon flux of 0.76×10^{-6} cnt/s/cm^2. Since these sources may be variable, they can be occasionally detected in shorter time segments, but not in a longer observation where the background is larger. Therefore, we have also considered the sum of the 3 HRC-I datasets, and the sum of the 2 ACIS-I, where we detect indeed 1 and 16 sources, respectively, not detected in the "all-summed" dataset. Our "combined-dataset" source list comprises therefore 206 individual X-ray detections.

The very deep Chandra image of NGC 2516, obtained from the sum of 3 HRC-I and 2 ACIS-I datasets, is shown in Figure 2. We note that had we included ACIS BI chips in this combined analysis we could not have obtained better results: these chips are characterized by a stronger background than the FI chips, that in the combined image would have hidden more sources than the possible new sources found due to the additional effective area.

3.3. Final X-Ray Source List

Having obtained detection lists for each dataset separately, and another detection list for the combined one (plus the additional detections from the 3 HRC-I datasets summed and the 2 ACIS-I datasets summed), we then combined them in a final detection list. The number of expected spurious detections is one per dataset, and since they are statistically independent (all but the sums), the total number of spurious detections should be 8-9. In doing this merging, we have applied shifts to the source positions from each dataset, computed as described in section 3.1.

A match between detections from different datasets was made whenever their distance was $d < 3\Delta r$ (where Δr is the *Pwdetect* computed positional error). In some instances this resulted in multiple matches, and we have then retained only those with the smallest distance (the rejected matches having $d > 1.5\Delta r$).

The resulting final source list is reported in Table 3 and comprises 284 unique detections. We report photon fluxes for the individual datasets (including the all-summed dataset), in units of 10^{-6} counts/s/cm^2, homogeneously for all detectors as explained. We include in the same Table the flux upper limit for sources undetected in a particular dataset. Entries in italics (either detections or upper limits) refer to sources falling in ACIS BI chips. Where an entry is missing the source fell outside the field of view of that particular dataset. As seen in the Table, in addition to the 206 detections in the combined dataset we find 2 more sources in ObsId 27 (HRC-I), 1 in ObsId 1405 (HRC-I), 1 in ObsId 999 (HRC-I), 8 in ObsId 65 (ACIS-I), 11 in ObsId 1229 (ACIS-S), 7 in ObsId 66 (ACIS-S), and 48 in ObsId 1458 (ACIS-23678). The large number of additional detections in ObsId 1458 arises largely because of its different pointing than the other datasets.

Table 3 forms the basis of a study of X-ray variability in NGC 2516, that will be the subject of a companion paper (Wolk et al. 2002). For the rest of this work, however, we will use average source fluxes and positions. We have computed weighted averages of positions and fluxes for all sources detected more than once, using the inverse square of the error as weight. The detected source flux in the combined dataset is itself a maximum-likelihood average, and it was further averaged with the flux in the datasets not in the combination (ObsIds 66, 1229, and 1458), when a source is detected also in these latter. The average for sources not in the combined-dataset list was made using detections in all datasets, but not including upper limits. However, including upper limits to compute a maximum-likelihood average flux would have changed little our results, since in most cases they are well compatible with the detected flux values. The resulting mean source fluxes and positions are listed in Table 4. In many cases, the uncertainty on source position is a fraction of arcsecond, thanks to the extremely narrow Chandra PSF.

3.4. X-Ray Source Fluxes

To convert X-ray count rates (or photon fluxes) to true fluxes, one needs to estimate a suitable conversion factor. Since the instrument effective area is already embodied in the derived photon fluxes, the conversion factor takes here the form of an "effective" photon energy. We have taken advantage of the availability of the ACIS spectra for many of our X-ray sources to estimate the spectral parameters of NGC 2516 stars. For all sources detected in ACIS FI chips, we have merged their extracted (background-subtracted) ACIS FI spectra, to compute color ratios with the best statistics. We have chosen three bands to compute two color ratios, namely 0.3-0.75 keV, 0.75-1.5 keV, and 1.5-8.0 keV. These were chosen with the purpose of maximizing the average number of counts in each band. We have defined color ratios as $CR_1 = 2.5\log(N_{cts}[0.75-1.5keV]/N_{cts}[0.3-0.75keV])$, and $CR_2 = 2.5\log(N_{cts}[1.5-8.0keV]/N_{cts}[0.75-1.5keV])$.

Using PIMMS, we have computed, in the $CR_1 - CR_2$ plane, a grid corresponding to Raymond-Smith single-temperature thermal models, with solar abundances, with different temperatures in the range $\log T = 6.0 - 7.8$ [K], and absorption in the range $N_H = 1 \cdot 10^{20} - 5 \cdot 10^{21}$ cm^{-2}. We find clearly that our color ratios cannot be reproduced using these models, for any choice of temperature and absorption, as was found by Jeffries et al. (1997) using ROSAT PSPC data. We have therefore tried with two-temperature Raymond-Smith models, where we have two more parameters: the temperature of the second component and its relative normalization. To reduce the parameter space, we have fixed the absorption to the value $N_H = 8.2 \cdot 10^{20}$ cm^{-2}, corresponding to the cluster extinction $A_V = 0.372$ (Jeffries et al. 2001). Moreover, the first temperature was set to $\log T = 6.5$ [K], a value usually found in two-temperature models of coronal sources of the same age (e.g. in the Pleiades; Gagné, Caillault and Stauffer 1995). Therefore, we have computed a grid analogous to the former, but now having as variables the second temperature and the component intensity ratio. In this case we find that most observed color ratios can be well reproduced, especially those with the smallest errors, and those of cluster members better than non-members (we discuss the identification of X-ray sources in Section 4). We have therefore adopted these two-temperature models to compute conversion factors for NGC 2516 coronal sources, using PIMMS.

In our sample there are 24 sources (among cluster members) with more than 50 counts in the combined ACIS FI spectra. Their position in the $CR_1 - CR_2$ plane is defined with small errors and thus we have computed for each of them individually a (second) temperature and component ratio, and therefore a conversion factor. For the remaining weaker detections and for upper limits (Section 4), the conversion factor was chosen as the median conversion factor of the stronger sources with the same spectral type. The derived higher temperatures are in the range $\log T = 6.87 - 7.60$ [K], and the high-to-low temperature component input count ratios are in the range $0.098 - 2.88$. The obtained conversion factors are in the range $2.42 \times 10^{-9} - 3.46 \times 10^{-9}$ ergs/count. (average photon energies in the range $1.51 - 2.16$ keV). Dividing this by the adopted ACIS-I spectrum-weighted on-axis effective area, we obtain the more usual count-rate to flux conversion factor, in our case in the range $8.46 - 12.1 \times 10^{-12}$ ergs/cm^2/count for ACIS-I, in very good agreement with Harnden et al. (2001). This translates into a flux for our weakest detected X-ray source of $\log f_X = -14.56$ (ergs/sec/cm^{-2}), in the band $0.1 - 4.0$ keV, that corresponds to a minimum X-ray luminosity, at the distance of NGC 2516, of $\log L_X = 28.69$ (ergs/sec). For non-member detections, we have adopted a conversion factor of 1.8 keV, and the lowest detected flux is $\log f_X = -14.66$ (ergs/sec/cm^{-2}). The minimum flux reached by Harnden et al. (2001) using a subset of these Chandra data was $\log f_X \sim -14.6$ (ergs/sec/cm^{-2}), and about the same value was reached by Sciortino et al. (2001) using XMM/Newton data. Earlier ROSAT studies had reached instead $\log f_X \sim -14.25$ (ergs/sec/cm^{-2}), or $\log L_X \sim 29.0$ (ergs/sec) (Jeffries et al. 1997), and $\log f_X \sim -13.95$ (ergs/sec/cm^{-2}), or $\log L_X \sim 29.3$ (ergs/sec) (Micela et al. 2000). The derived X-ray luminosities for the detected NGC 2516 members (identified with their Jeffries et al. 2001 number in column "Star#") are listed in Table 5. From the range of conversion factors found, we estimate that the uncertainty on L_X due to an inappropriate spectral model is at most 40%, and more typically 12% (rms).

Table 5: X-Ray Luminosities for Detected NGC 2516 Members

Nr.	Star#	$\log L_x$ (ergs/s)	Nr.	Star#	$\log L_x$ (ergs/s)	Nr.	Star#	$\log L_x$ (ergs/s)	Nr.	Star#	$\log L_x$ (ergs/s)
1	4125	30.33	67	7678	29.74	128	8935	29.59	183	10894	29.58
2	4598	30.30	69	7690	29.15	129	8967	29.75	185	11082	29.53
3	15496	29.79	71	7743	29.85	130	8969	29.07	186	11233	30.18
4	5024	29.62	72	7782	29.77	131	8991	29.24	188	11485	29.46
5	5052	30.09	76	7864	30.11	132	8997	29.91	190	5899	29.48
6	5061	29.90	78	15503	29.36	133	9025	28.99	193	7276	29.08
8	5957	29.99	81	7937	28.94	134	9035	29.06	201	9402	29.06
9	6029	29.99	83	7959	29.44	135	9048	28.85	202	10017	29.24
10	6106	29.34	84	7962	29.11	137	9054	30.03	203	10348	28.96
13	15499	29.79	85	7967	29.25	138	9061	29.02	204	10871	29.30
14	6268	29.38	89	8036	29.37	140	9140	30.05	211	5446	29.47
15	6263	29.19	90	8047	29.01	141	9153	29.35	212	6264	29.10
16	6373	29.58	91	15534	29.25	143	9175	29.83	214	6751	29.06
17	6452	29.40	92	8099	29.77	144	9185	29.31	215	7260	29.19
20	6492	29.36	94	15504	29.76	145	9202	29.07	218	4105	30.25
22	6570	29.21	95	8172	29.18	146	9283	28.87	221	5862	29.37
23	6603	29.25	96	8192	29.26	147	9286	28.95	222	6049	29.33
24	6605	29.20	97	8261	29.37	149	9328	29.58	223	6070	29.43
26	6640	29.14	100	8332	29.36	150	9361	29.06	225	6508	28.94
27	6649	29.94	101	8404	29.02	152	9465	30.07	226	7590	29.01
29	6689	29.89	102	8408	29.23	154	9486	30.03	243	11240	29.55
32	6852	29.16	106	8458	30.09	155	9512	29.16	246	7358	29.33
33	15500	29.88	107	8502	29.07	156	9676	30.02	252	7194	29.03
34	7001	29.45	108	8529	29.92	158	15509	30.53	254	7312	28.87
35	7104	29.35	110	8536	28.98	159	15508	30.47	256	7454	28.91
37	7120	28.70	111	8556	28.94	161	9835	30.00	259	7619	29.35
40	7203	28.90	114	15506	29.79	162	9852	29.52	262	8037	29.71
42	7231	29.55	115	8634	30.05	163	9882	29.84	264	8126	29.06
44	15501	29.44	116	8645	30.01	164	9908	29.64	266	8289	28.75
47	15519	28.97	117	8647	28.69	165	10010	29.14	268	8328	28.87
51	7419	29.05	118	8654	29.08	166	10040	29.63	270	8411	28.86
52	7420	29.25	119	8660	29.93	167	10046	30.01	273	8584	29.39
55	7505	28.72	120	8737	28.74	169	10047	29.75	275	8641	29.14
58	7553	29.15	121	8776	28.92	170	10143	30.07	277	8689	28.95
60	7585	30.13	123	8893	29.71	175	10471	29.84	278	9015	28.87
61	7595	29.45	124	8886	29.78	178	10702	29.18	282	9513	29.01
64	7622	29.16	125	8920	28.85	180	10754	29.17	283	9655	28.97
65	7650	29.57	126	8923	28.84	181	15510	30.01	284	9696	28.96
66	7667	29.86	127	8932	28.84	182	10863	29.40			

4. Optical Identifications

In Table 4 we also list optical counterparts to all detected X-ray sources. We have used the optical catalog of Jeffries et al. (2001), complete to about V=20, supplemented by a list of brighter stars, as reported by Jeffries et al. (1997). The Jeffries et al. (2001) catalog number is reported in Table 4 (column "Star#"). We have identified an X-ray source with an optical star when their distance is $d < 3\Delta r$ (but always $d < 25''$ to avoid many spurious matches in the outer parts of the field of view), to which we have added identifications within $d < 4''$ (but not exceeding $d < 5.5\Delta r$), to allow for residual errors, especially for brighter optical stars (whose optical positions are less accurate) and X-ray sources with very few counts, whose true positional error is underestimated. In doing this, we have also found (and corrected) a systematic offset between optical and X-ray positions of $0.07''$ in RA and $0.19''$ in Dec for stars in Jeffries et al. 2001 (slightly larger values of $0.68''$ and $0.59''$ were found for the brighter stars).

In this way, we find that 23 X-ray sources have more than one optical counterpart. Inspecting visually each of these cases, we have found that for most of them one star was a much closer match (within $d < 1.5\Delta r$) than any other candidate counterpart. Therefore, in cases of multiple counterparts we have restricted the matching distance to $d < 1.5\Delta r$. This leaves four X-ray sources with double optical identification (one member and one non-member for each), with no obvious choice between the two counterparts. These are listed each as two separate rows in Table 4. We have taken the membership information from Jeffries et al. (2001).

To summarize, among the 284 unique X-ray sources we have detected in the NGC 2516 field, we have identified 211 with at least one optical star. There are 155 cluster members associated with an X-ray source, and 60 non-members associated with an X-ray source (the two numbers sum up to 211+4, the latter being the number of doubly-identified sources). There remain 73 X-ray sources without an optical identification with our optical catalog stars. In addition to the detected cluster members, in our combined Chandra field of view fall another 570 cluster members not detected in X-rays. Since the total number of members is 1298, there are 573 more members outside our surveyed region. For each of the 570 members that were observed but not detected in any dataset, we have computed flux upper limits with *Pwdetect*, in both individual datasets and the all-summed dataset. We have then taken the lowest value among the various datasets. The L_X upper limits for the undetected cluster members are listed in Table 6.

Taken at face value, we have detected 155/725 cluster members, or 21.4%. However, we caution that our point-source sensitivity varies strongly across the field of view, being much larger near the center, and that Jeffries et al. (2001) estimate some non-member

Table 6: Upper Limits to X-Ray Luminosities for Undetected NGC 2516 Members

Star#	$\log L_x$ (erg/s)	Star#	$\log L_x$ (erg/s)	Star#	$\log L_x$ (erg/s)	Star#	$\log L_x$ (erg/s)	Star#	$\log L_x$ (erg/s)
1531	30.57	3278	30.26	3961	30.18	4836	29.76	5530	29.38
1645	30.37	3301	30.05	4000	29.94	4840	29.87	5533	29.41
1657	30.41	3387	30.27	4003	30.23	4842	29.87	5536	30.31
1753	30.59	3397	30.15	4046	29.95	4855	29.73	5563	30.27
1781	30.39	3402	30.01	4069	29.84	4889	29.78	5573	29.29
1798	30.44	3406	30.16	4072	29.80	4911	30.43	5576	29.59
1830	30.78	3407	30.28	4089	30.02	4914	29.97	5581	29.80
1832	30.73	3433	30.16	4113	29.91	4915	30.38	5586	29.97
1834	30.55	3440	30.06	4126	30.02	4936	29.75	5626	29.72
1859	30.29	3468	30.64	4146	29.87	5010	29.65	5631	29.64
2026	30.48	3550	30.05	4166	30.51	5018	29.91	5678	29.98
2047	30.59	3577	30.08	4187	29.91	5029	30.22	5685	29.85
2057	30.52	3598	30.28	4229	29.81	5066	29.66	5741	30.25
2146	30.34	3614	30.07	4254	29.77	5079	29.55	5785	29.53
2208	30.39	3621	30.09	4273	30.17	5088	29.77	5833	29.31
2231	30.24	3624	30.10	4322	29.75	5104	30.45	5835	29.38
2233	30.16	3631	30.02	4364	29.86	5107	29.96	5836	29.37
2277	30.49	3648	30.14	4397	29.79	5110	30.40	5843	29.70
2294	30.23	3651	30.20	4404	30.02	5130	29.71	5849	30.01
2306	30.43	3676	30.01	4432	29.79	5144	29.86	5871	29.88
2380	30.01	3680	30.07	4448	29.81	5169	30.42	5875	29.20
2437	30.14	3688	29.96	4473	29.80	5175	29.61	5876	29.21
2462	30.20	3730	29.99	4479	29.73	5179	29.42	5877	29.37
2525	30.42	3748	30.23	4530	29.80	5193	29.40	5878	30.12
2534	30.43	3757	30.22	4538	30.41	5210	30.36	5882	29.20
2606	30.27	3777	29.90	4552	30.00	5243	29.75	5887	29.37
2623	30.05	3780	30.01	4560	29.74	5261	29.57	5901	29.36
2661	30.25	3795	30.08	4574	29.88	5262	29.42	5904	29.99
2797	30.37	3807	29.92	4576	30.52	5280	29.45	5911	29.24
2801	30.08	3819	30.17	4606	29.96	5285	29.76	5972	30.25
2844	30.40	3845	30.04	4647	29.76	5299	29.89	5989	29.12
2867	30.10	3856	29.97	4648	29.92	5312	29.67	5991	29.61
3170	30.06	3876	30.08	4656	30.14	5363	29.96	6027	29.84
3186	29.93	3886	29.98	4718	29.92	5429	29.65	6036	29.87
3208	30.15	3887	29.95	4727	29.69	5499	29.77	6044	29.78
3219	30.11	3891	29.88	4750	29.96	5509	29.28	6057	29.90
3245	30.17	3942	29.87	4760	29.92	5526	29.64	6077	29.82
3273	30.26	3958	30.19	4808	29.62	5528	30.18	6095	29.30

Table 6: Upper Limits to X-Ray Luminosities for Undetected NGC 2516 Members (continues)

Star#	$\log L_x$ (erg/s)	Star#	$\log L_x$ (erg/s)	Star#	$\log L_x$ (erg/s)	Star#	$\log L_x$ (erg/s)	Star#	$\log L_x$ (erg/s)
6096	29.73	6705	28.91	7480	29.98	8242	29.26	8999	29.74
6111	29.92	6724	29.51	7483	28.59	8256	30.31	9058	29.17
6112	30.21	6725	29.81	7501	30.22	8262	29.19	9079	29.27
6152	29.23	6733	29.66	7504	29.28	8298	28.88	9088	30.01
6160	30.30	6745	29.86	7542	30.22	8313	29.17	9146	29.08
6177	29.82	6771	28.79	7548	28.66	8320	29.80	9214	29.66
6180	29.28	6796	29.03	7559	28.70	8340	28.51	9241	29.24
6204	29.26	6847	28.94	7586	30.35	8359	28.87	9243	29.81
6209	30.17	6871	29.59	7596	29.85	8370	28.87	9259	28.69
6222	30.17	6880	28.98	7599	30.14	8385	29.71	9270	29.30
6238	29.05	6912	29.50	7613	30.24	8391	28.81	9297	30.11
6245	29.75	6940	28.78	7628	29.37	8394	29.79	9346	30.08
6265	29.72	6942	28.91	7666	29.17	8397	29.63	9415	29.04
6289	29.75	6949	29.35	7682	29.50	8401	28.71	9446	29.15
6297	30.34	6963	28.83	7710	29.92	8453	29.64	9453	29.25
6301	29.80	6965	29.43	7721	29.45	8462	28.62	9459	30.23
6322	29.59	6970	29.16	7734	29.51	8465	28.80	9475	29.00
6323	29.78	6976	29.55	7771	28.82	8479	28.64	9572	29.06
6342	29.68	6996	29.66	7788	28.89	8509	29.26	9596	29.01
6377	29.75	7006	29.07	7806	29.45	8518	30.36	9659	29.04
6391	29.77	7028	29.40	7813	29.92	8524	28.83	9684	29.92
6401	30.24	7036	29.47	7838	28.63	8531	28.63	9700	29.85
6402	28.98	7038	29.81	7842	29.85	8591	28.73	9703	28.94
6426	29.52	7041	28.90	7870	28.49	8603	29.90	9721	30.35
6445	29.02	7051	29.20	7900	30.22	8665	29.51	9727	29.54
6446	29.32	7113	29.47	7918	29.19	8675	29.54	9791	29.38
6465	29.78	7154	28.64	7932	29.14	8678	28.80	9811	29.28
6473	29.20	7189	28.77	7941	29.66	8714	28.77	9875	29.03
6501	29.08	7206	28.71	7984	29.80	8716	30.44	9878	29.98
6514	29.71	7207	29.07	7985	29.96	8727	28.83	9885	29.65
6575	29.19	7259	29.99	8031	28.65	8793	29.52	9911	29.73
6577	29.22	7322	28.99	8033	30.38	8801	28.65	9939	29.04
6594	29.09	7335	29.65	8055	28.84	8827	28.74	9959	29.24
6628	29.26	7347	29.64	8058	28.52	8917	28.77	9961	29.02
6650	29.32	7352	29.58	8132	28.88	8947	28.99	10077	29.12
6676	29.03	7430	29.81	8138	28.47	8949	29.53	10129	29.31
6683	29.59	7442	30.13	8166	28.93	8989	29.47	10132	29.07
6691	29.66	7443	28.60	8219	30.27	8990	28.81	10152	29.76

Table 6: Upper Limits to X-Ray Luminosities for Undetected NGC 2516 Members (continues)

Star#	$\log L_x$ (erg/s)	Star#	$\log L_x$ (erg/s)	Star#	$\log L_x$ (erg/s)	Star#	$\log L_x$ (erg/s)	Star#	$\log L_x$ (erg/s)
10162	29.14	10857	29.50	11615	30.34	12302	29.96	13349	30.39
10191	29.14	10868	30.38	11634	30.31	12309	30.41	13581	30.39
10210	29.13	10877	29.28	11713	29.52	12356	30.37	13648	30.09
10281	29.90	10884	29.72	11716	29.41	12362	29.97	13760	30.02
10284	30.28	10902	29.82	11718	29.49	12365	30.20	13861	30.07
10293	29.70	10929	29.29	11729	29.49	12404	29.76	13900	30.49
10298	29.13	10957	29.97	11750	29.63	12416	30.21	15497	29.79
10301	29.85	11014	29.65	11782	30.09	12451	29.62	15498	29.88
10330	29.27	11029	29.27	11788	29.52	12472	30.44	15502	29.00
10365	29.24	11031	30.25	11813	29.83	12543	29.85	15505	29.05
10370	30.25	11039	29.61	11823	29.83	12553	29.98	15507	28.93
10398	30.27	11060	29.21	11844	29.45	12565	30.19	15514	29.86
10401	30.24	11129	29.49	11852	29.44	12597	30.23	15515	29.69
10434	29.96	11132	29.75	11857	29.59	12600	29.76	15517	29.04
10440	29.86	11136	29.99	11867	29.92	12613	29.64	15518	29.54
10452	29.12	11142	29.74	11876	30.37	12621	30.27	15519	29.48
10505	30.02	11153	29.33	11906	29.48	12628	30.19	15520	28.82
10527	29.78	11162	30.34	11956	29.41	12649	30.20	15521	28.90
10547	29.16	11195	29.29	11969	30.26	12709	29.98	15522	29.01
10588	29.57	11231	29.64	11970	29.92	12711	29.68	15524	28.76
10594	30.20	11235	29.97	11978	30.35	12728	30.18	15525	29.39
10605	29.56	11243	29.39	11982	30.19	12754	29.65	15526	28.74
10606	30.28	11253	29.63	11983	29.67	12802	29.81	15527	28.68
10667	29.91	11287	29.36	11998	29.95	12805	30.01	15528	28.89
10688	29.61	11303	30.24	12005	29.55	12814	30.41	15529	28.73
10695	29.40	11304	29.41	12067	30.30	12835	30.19	15530	28.74
10723	29.17	11307	29.40	12089	29.65	12868	29.74	15531	29.79
10735	29.60	11332	30.28	12109	30.29	12874	30.26	15533	29.06
10736	29.92	11348	29.44	12118	29.99	12903	30.45	15534	29.42
10753	29.29	11363	30.15	12134	29.56	12909	30.09	15535	29.87
10760	29.69	11372	29.39	12147	30.33	13013	30.06	15536	29.99
10768	29.20	11405	30.17	12201	29.60	13065	30.06	15538	29.88
10783	30.24	11441	29.89	12206	29.88	13079	30.07	15539	29.94
10796	29.28	11451	29.60	12210	30.14	13168	30.20	15541	28.54
10811	30.19	11520	29.40	12216	30.29	13174	29.97	15542	30.18
10817	29.95	11549	29.44	12235	30.31	13182	30.16	15543	29.65
10832	29.92	11556	29.44	12244	30.20	13273	30.43	15544	28.86
10848	29.24	11611	29.86	12276	29.93	13342	30.33	15545	29.02

contamination in their candidate-member catalog, increasing towards the outer parts (i.e. over a large area, where our X-ray sensitivity is poor). This explains in part why this detection fraction is apparently so different than the value of about 42% found by Harnden et al. (2001), who analyzed a subset of the X-ray data used here, considering only the cluster central region (in the same region we find a detection rate of 33.5%), since their input optical catalog (going down to $V \sim 19$) was less complete than the Jeffries et al. (2001) catalog (down to $V \sim 21$), and thus results in 198 observed members in the central region, instead of our 251 observed members. The detailed detection rate for members of various spectral types are reported in Table 7. In this table, the sum of numbers in column "Nr.Undet." is 568, and not 570, since we have left out two (undetected) red giants, that are also cluster members according to Dachs (1970). A third red giant member was not observed by us. We note that for all spectral types our detection fraction is lower than 50%. Since optical spectra are not available for most NGC 2516 members, we have assigned spectral types from $B - V$ and $V - I$ optical colors, as listed in the same Table, corrected for the average cluster reddening $E(B - V) = 0.12$.

We show in Figure 3 the color-magnitude diagrams for NGC 2516 members, and detected non-members, using $B - V$ and $V - I$ colors, respectively. The cluster binary sequence is visible, and was discussed by Jeffries et al. (2001). We can see that our detected cluster members span the whole range of colors down to the reddest part of the diagrams. There seems to be a limit around $V \sim 20$, $V - I \sim 3$ to the detected members in the color-magnitude diagram, and this is probably caused by the sensitivity threshold of the X-ray observations. Assuming an X-ray flux threshold $\log f_X \geq 10^{-14.56}$ (ergs/sec/cm^{-2}), and a bolometric correction $BC = -2.65$, this implies $\log L_X/L_{bol} \geq -3$. This corresponds to the most active dMe stars, and therefore we do not expect to detect in X-rays cluster members fainter than this limit. Some of the non-members fall far above the cluster main sequence (but are not cluster giants), and are therefore probable foreground low-mass field stars. A slightly larger number of non-members fall below the cluster main sequence, and are therefore probable background objects, either active stars or reddened AGNs.

Taking into account the identification radius used for each X-ray source, we have computed the total area searched for matches. Comparing it to the spatial density of stars in the central $10' \times 10'$, we find that the expected number of chance coincidences is 6.9 for members, and 29 for non-members. Among members, spurious optical identifications are probably among the redder, fainter stars; for non-members, they should be in the "clump" at $V \sim 18 - 20$ and $V - I \sim 1$ (see Jeffries et al. 2001). Therefore, our subsample of detected members can be considered nearly free of identification ambiguities, while substantial ambiguities exist for the non-member detections, which will be paid little attention in the following.

As for the 73 X-ray sources without identification in the Jeffries et al. catalog, we expect that the 8-9 predicted spurious X-ray detections are to be found preferentially among them (the weakest detections fall indeed in this group). We have therefore visually checked if they are real X-ray sources. While some of them may be spurious, many are certainly not. Then, we have examined visually their position on the DSS red images. For 42 of them, there is indeed no visible counterpart down to the plate limit. There are then 10 undefined cases, falling mostly over halos of bright optical stars. Eleven sources have a faint optical star-like counterpart, and another 10 sources have a very faint counterpart, very near to the noise limit (some may indeed be noise). These objects may either be cluster members or unrelated background objects, perhaps extragalactic.

Jeffries et al. (2001) discuss the completeness of their optical catalog, and they expect to be 98% complete down to $V = 19$, and 90% complete for $19 < V < 20$. Therefore, having 155 X-ray detected cluster members, mostly with $V < 19$, we expect about 3 to 10 to be missing in the optical catalog. These objects are probably found among those near bright stars, or those with faint DSS counterparts. From the Chandra deep-survey $\log N - \log S$, and the sensitivity map computed using *Pwdetect* on our combined dataset, we estimate that 19 to 26 extragalactic sources (using the models of Giacconi et al. 2001, and Tozzi et al. 2001, respectively) should be detected in our NGC 2516 fields.

Table 7: Detection Statistics for Different Spectral Types

Spec. Type	Color Range	Nr. Det.	Nr. Undet.	Detect. Rate (%)	Median $\log L_X$ (erg/s)	Mean $\log L_X$ (erg/s)
B	$(B-V)_0 < 0.0$	12	26	31.6	<28.54	29.00
dA	$0.0 \leq (B-V)_0 < 0.3$	12	46	20.7	<28.51	28.88
dF	$0.3 \leq (B-V)_0 < 0.5$	19	25	43.2	29.40	29.41
dG	$0.5 \leq (B-V)_0$, $(V-I)_0 < 0.93$	38	77	33.0	29.06	29.18
dK	$0.93 \leq (V-I)_0 < 2.2$	52	175	22.9	29.02	29.07
dM	$2.2 \leq (V-I)_0 < 5.0$	22	219	9.1	28.69	28.74

5. Results

5.1. NGC 2516 X-Ray Luminosity Functions

We have computed maximum-likelihood X-ray luminosity functions for all NGC 2516 members observed in our Chandra survey, including upper limits, using ASURV (Feigelson and Nelson 1985). We show in Figure 4 these X-ray luminosity functions, separately for the various spectral types. In the same Figure, we compare the results obtained for NGC 2516 with those obtained for the Pleiades cluster by Micela et al. (1999) using ROSAT HRI data. The Pleiades X-ray luminosities were computed in the band 0.1 − 2.4 keV, but for the adopted spectral model only a small upward correction (3-7%) would be needed to convert them to the band 0.1 − 4.0 keV. The median and mean X-ray luminosities L_X obtained for each spectral types in NGC 2516 are also reported in Table 7. Since we have detected less than 50% of observed members for all spectral types, in some cases (B and A stars) we have only obtained an upper limit on the median L_X.

The B-star X-ray luminosity function spans the widest interval among all spectral types, reaching the highest L_X value found in NGC 2516, or $\log L_X = 30.53$ (ergs/sec), and also going down to the lowest detected L_X values and below, with many stars undetected with upper limits lower than $\log L_X = 29.0$ (ergs/sec). The emission of the two X-ray brightest B stars cannot therefore due to lower-mass companions, but must be intrinsic to the massive stars themselves (of types B9.5V and B2IVnpe, respectively), as concluded already by Jeffries et al. (1997), and probably due to shocks in the stellar wind, as usually found in OB stars.

The A-star X-ray luminosity function spans instead a range similar to the luminosity functions of later-type stars, and is compatible with an X-ray emission uniquely due to lower-mass companions. A stars have the second lowest detection rate in our NGC 2516 survey (see Table 7); only M stars have a lower detection fraction, due to both their intrinsic X-ray faintness and to strong non-member contamination in their optical catalog. However, NGC 2516 is remarkable in having a number of chemically peculiar A stars as members. We have observed 8 of them, and detected 6 or 7 (because of the unresolved double CPD-60 944), namely one half of our detected A stars are chemically peculiar. Therefore, either there is a connection between chemical peculiarity and binarity, such that peculiar stars are more often binaries than non-peculiar stars, and the X-ray emission comes from the companions, or rather a connection exists between chemical peculiarity and X-ray activity intrinsic to the A stars themselves, without emission from companions. This is likely to happen if these peculiarities go as far as to modify the structure of the outer layers of the star, e.g. changing the opacity, and turning convection on (many such stars are known to possess strong surface magnetic fields; Borra, Landstreet and Mestel 1982). Drake et al. (1994) have also found evidences of strong X-ray emission from chemically peculiar early-type stars. In NGC 2516, the very high X-ray detection rate of chemically peculiar A stars, especially compared to the low detection rate of normal A stars, is an intriguing result that surely deserves careful separate investigations.

Among the three red giants belonging to NGC 2516, two are in our observed sample, but neither was detected. The first of these stars has $V = 6.71$, $B - V = 1.28$, and $\log L_X < 28.73$ (ergs/sec), and the other $V = 5.19$, $B - V = 1.76$, and $\log L_X < 29.99$ (ergs/sec). They are not included in the X-ray luminosity functions discussed below.

As shown in Table 7, the F stars in NGC 2516 have both a median L_X and a detection fraction larger than other spectral types. For this reason, we can conclude that the X-ray emission of F stars is very probably intrinsic, and not due to companions. For later types, we see a steady decrease in the median L_X towards lower masses. In Figure 4 we see also that for G and K stars the NGC 2516 luminosity functions stay distinctly below the corresponding luminosity functions for the Pleiades, a result similar to that found by Jeffries et al. (1997), Harnden et al. (2001) and Sciortino et al. (2001), but with better detection statistics. For M stars, we find a slightly lower luminosity function with respect to the Pleiades, analogously to Sciortino et al. (2001), while Harnden et al. (2001) derived a luminosity function very similar to the Pleiades. Jeffries et al. (1997) argued that the lower activity level in NGC 2516 was probably due to its lower metallicity compared to the Pleiades, and discuss how metallicity can lower X-ray activity especially during some evolutionary phases. A more recent work (Terndrup et al. 2002), however, seems to rule out a subsolar metallicity for NGC 2516, so that this cannot anymore be a valid explanation for the observed lower activity levels in NGC 2516. Although NGC 2516 is older than the Pleiades, it is unclear if the observed, fairly strong, decrement in the average X-ray luminosities can be uniquely attributed to an age difference. Nor is the age-activity relation without exceptions, as is shown by the Hyades and Praesepe clusters, having the same age but different X-ray luminosity functions. Thus, NGC 2516 might be another discrepant case with respect to the average age-activity relation. Before drawing such a conclusion, however, we must still ascertain whether some bias affects the X-ray luminosity functions just derived for NGC 2516. One such bias might easily be the contamination by non-members in the optical catalog. The magnitude of such a contamination was estimated by Jeffries et al. (2001), and we try to eliminate its effect on the X-ray luminosity functions in the next section.

5.2. Non-Members Contamination

We assume that contaminating non-members are found among undetected stars in the optical NGC 2516 catalog, since X-ray detected candidate members can be considered confirmed members. Jeffries et al. (2001) tabulate estimates of the non-member contamination fraction affecting their catalog, separately for different $V-I$ ranges, and for single and binary stars, respectively. On this basis, we have computed, for each stellar color/type range, the number of expected contaminants, and therefore the probability p_m that a star is actually a member. A given upper limit was then included in the luminosity function if, taking a random number from a uniform distribution between 0 and 1, this was smaller than the membership probability p_m for that star. This procedure was repeated 200 times for each luminosity function, again separately for different spectral types (Figure 5). These simulated luminosity functions should be a good estimate of the true, contamination-free NGC 2516 luminosity function. A few caveats apply, however: the Jeffries et al. (2001) contamination estimates are average over the whole optical survey. The contamination is lower near cluster center and higher outside our X-ray surveyed region, therefore our correction may be slightly overestimated.

In Figure 5 we see that the correction is negligible for F stars, whose contamination is expected to be very small. For G stars the correction is more noticeable, and the G-star NGC 2516 luminosity function may even cross that of the Pleiades around $\log L_X = 30$ (ergs/sec). Its median value, however, remains lower, albeit by only 0.13 dex. Also in K stars, the discrepancy with the Pleiades is slightly reduced with respect to the uncorrected case, but it remains very evident, and in fact the largest among all spectral types. A set of two-sample Wilcoxon tests, applied to the Pleiades and to each of the simulated luminosity functions, gives a distribution of probabilities of not being drawn from the same population, with median value $P_{50} = 0.885$, 18% quantile $P_{18} = 0.884$, and 82% quantile $P_{82} = 0.891$, for F stars. For G stars, we obtain $P_{50} = 0.954$, $P_{18} = 0.921$, and $P_{82} = 0.971$, and for K stars $P_{50} = 0.999$, $P_{18} = 0.998$, and $P_{82} = 0.999$. Therefore, only in the case of K stars are the NGC 2516 and Pleiades luminosity functions different more significantly than 99.7% (3 sigmas).

In NGC 2516 M stars the contamination is large, and the correction to the luminosity function quite relevant. The corrected median L_X may even be the same as the Pleiades, and the whole luminosity function of NGC 2516 M stars does not differ substantially from that of Pleiades M stars. A Wilcoxon test gives $P_{50} = 0.962$, $P_{18} = 0.942$, and $P_{82} = 0.978$, a not very significant difference. Qualitatively, this is the same result found by Micela et al. (2000) using ROSAT HRI data, and by Harnden et al. (2001) using a subset of our Chandra data.

The median and mean values of the L_X distributions corrected for contaminations are listed in Table 8.

We conclude that, at least in the case of K stars, there is a definite lower X-ray activity level in NGC 2516 with respect to the Pleiades, that cannot be ascribed to contamination by stars not belonging to the cluster. If Jeffries et al. (2001) underestimate the optical contamination, however, the X-ray luminosity functions move towards higher values, and become more similar to the Pleiades. An underestimate by a factor of 2 would result in a probability of difference of $P_{50} = 0.766$ for the G stars, of $P_{50} = 0.977$ for the K stars, and of $P_{50} = 0.730$ for the M stars.

We have also investigated how much these results depend on the assumed distances for NGC 2516 and the Pleiades. For these latter, we have adopted a distance of 127 pc, as in Micela et al. (1999). The NGC 2516 distance used here, 387 pc, is the same used by Jeffries et al. (1997), and coincides also with that derived by Terndrup et al. (2002) from variable-metallicity isochrone fitting. For both clusters, the Hipparcos distances are smaller: 116 pc for the Pleiades (Mermilliod et al. 1997), and 346 pc for NGC 2516 (Robichon et al. 1999). If we adopt the Hipparcos distances for both clusters, then their X-Ray luminosity functions shift towards lower values by 0.079 dex for the Pleiades, and by 0.097 dex for NGC 2516, respectively. Therefore, they become more similar for F stars, and more different for G, K, and M stars. The contamination-corrected probabilities of difference P_{50} for G, K, and M stars now become 0.976, 0.99956, and 0.984, respectively. Again, the only very significant difference occurs for K stars. If a fixed metallicity value for NGC 2516 (from spectroscopy) is instead used, Terndrup et al. (2002) derive a larger distance of 407 pc. Using this distance value (and assuming 127 pc for the Pleiades), the NGC 2516 luminosity functions move upwards by 0.045 dex. In this case, the F-star luminosity functions become more different, and those of G, K, and M stars more similar. The contamination-corrected probabilities of difference P_{50} for G, K, and M stars are in this case 0.842, 0.985, and 0.840, respectively, and the K-star difference becomes thus only marginally (2.44σ) significant. This larger distance value for NGC 2516 might be unreliable, however, being incompatible at the 2.5σ level with the Hipparcos distance (Terndrup et al. 2002), while the value of 387 pc, used in this paper, is well compatible with the Hipparcos value.

Table 8: Contamination-Corrected Average X-Ray Luminosities

Spectral Type	Median $\log L_X$ (erg/s) Quantiles			Mean $\log L_X$ (erg/s) Quantiles			Prob. Diff. w.r.t. Pleiades		
	18%	50%	82%	18%	50%	82%	18%	50%	82%
dF	29.40	29.40	29.40	29.41	29.41	29.41	0.884	0.885	0.891
dG	29.16	29.16	29.19	29.23	29.25	29.27	0.921	0.954	0.971
dK	29.07	29.08	29.08	29.13	29.14	29.15	0.998	0.999	0.999
dM	28.70	28.72	28.72	28.77	28.78	28.80	0.942	0.962	0.978

5.3. X-Rays and Binarity

In the color-magnitude diagram of NGC 2516, a binary sequence is easily identifiable (Figure 3), and on this basis Jeffries et al. (2001) have assigned a binarity flag to photometric NGC 2516 members. By definition, the binary sequence comprises only near-equal-mass systems ($q > 0.6$), so that more binaries with larger mass ratios are left among the apparently single stars.

We have examined whether the NGC 2516 binaries have an enhanced emission with respect to single stars, that may be due to some interaction between close components, as in well known active binaries. The detection rate of F and G binaries (taken together to augment their statistics) is of 18/55=0.327, while the rate for single F and G stars is 39/104=0.375. For K binaries the rate is 14/58=0.241, while for single K stars is 38/169=0.225. Therefore, differences between detection rates of singles and binaries of the same type are negligible. This is surprising, since if there is a given probability P_1 of detecting a single star of a given type, the probability of detecting at least one star in a pair, of the same type, should be larger: $P_2 = 1 - (1 - P_1^2) = P_1(2 - P_1)$. Thus, in the case of K binaries one would expect a detection fraction of 0.40. A possible explanation for this apparent lack of detected binaries might be a different contamination fraction for singles and binaries, respectively. Also a different spatial distribution might produce the same effect, if for example the binaries are less concentrated towards the center, and thus observed at large offaxis angles (and therefore lower sensitivity) in our X-ray datasets; however, the mean distances from cluster center of singles and binaries are $17.7'$ and $19.2'$, respectively, and their small difference seems not enough to account for the observed effect. On the contrary, mass segregation (confirmed by Jeffries et al. 2001) would lead us to expect more binaries near the center. A better explanation may be that the singles are not actually singles, and companions with much lower optical luminosity contribute a non-negligible fraction to the detected X-ray flux. In fact, using field stars q distributions Jeffries et al. (2001) estimated the total percentage of binaries in NGC 2516 to be high ($\sim 85\%$), although probably no higher than in the Pleiades.

It is also interesting to study the luminosity functions of binary vs. single stars, as we show in Figure 6 separately for F, G stars and for K stars. We plot the binary star function, the single star function (both corrected for contamination), and the convolution of the latter with itself, simulating a binary star luminosity function. The observed F, G binary luminosity function crosses the simulated binary luminosity function, with a high-activity tail independent of any contamination correction. This is probably due to close binaries, making up a sizable fraction of our binary sample, that have not yet slowed down their rotation (as single F,G stars have done), and are therefore more active than either wide binaries or pairs of single stars.

In the case of K stars, the contamination correction is critical to bring the observed binary star luminosity function close to the simulated one. If the largest correction is adopted, the observed and simulated binary stars luminosity functions are very similar, suggesting that binarity does not affect X-ray emission. On the contrary, if no correction is made one would conclude that K binaries are underactive with respect to single K stars. This might not be real, however, but simply caused by singles not being actually so, but in many cases binaries with large mass ratios. We conclude that, at most, K binaries in NGC 2516 are only slightly underactive with respect to their single counterparts.

In the Pleiades, the X-ray luminosity function of binary G stars is consistent with the convolution of that of single G stars with itself (Micela et al. 1996), and the same is found for K stars. Binary stars in the Pleiades are known much better than in NGC 2516, and our findings do not rule out that binaries in NGC 2516 behave in the same way as Pleiades binaries (apart from the high-activity tail in the NGC 2516 F,G binaries). In the older Hyades, Pye et al. (1994) found the opposite effect for dK stars, namely long-period binary stars are significantly more active than pairs of single dK stars, a behavior that we can rule out for NGC 2516 dK stars.

5.4. Relationships between X-Ray and Optical Properties

In addition to the study of color-dependent X-ray luminosity functions, we have examined possible further relationships between X-ray emission and optical colors (hence stellar mass). Plots of $\log f_X/f_V$ versus $V-I$ are shown in Figure 7a and b, for members and non-members respectively. As observed in other clusters, there is a clear trend of increasing $\log f_X/f_V$ from the bluest to the reddest colors (Figure 7a). In this Figure, the most massive stars are not included since we lack their $V-I$ colors. The total observed range of $\log f_X/f_V$ (including the massive stars) is $[-5.35, +0.066]$. Values of $\log f_X/f_V \sim 0$ are rather extreme, and attained only by a few flaring M stars; more common "high" values of $\log f_X/f_V$ cluster around $\log f_X/f_V \sim -1$, also attained by the latest-type (dM) stars in our sample. The low $\log f_X/f_V$ values that we observe for the most massive stars are also in agreement with those typical of B stars. For a given color, there is a large spread, by one order of magnitude or more, as is especially evident for G-early K stars ($V-I \sim 1$). Upper limits are in most cases consistent with the distribution of detections, and do not imply a different population of low-activity stars.

Since both $V-I$ and $\log f_X/f_V$ are (to a first approximation) distance-independent quantities, we can meaningfully compare their distribution for members and non-members. We have selected in Figure 7a a region where all cluster members are found, and have over-plotted this region in Figure 7*b*. Here we see that some objects fall in the same region as cluster stars, and are therefore compatible with coronally active, probably young stars (some of them might actually be misclassified real cluster members). Young active stars are expected to be found around this sky direction, belonging to the Gould Belt (Guillout et al. 1998). Other objects are either over- or underluminous in X-rays for their optical colors, and they may be distant AGNs or nearby unactive stars, respectively (or simply spurious identifications). This diagram may help to reject spurious identifications with cluster members (that however seem not to be present in our sample), but cannot be used to select new cluster members blindly, without risking to include coronally active stars not belonging to the cluster. One possible exception is that of stars passing the color-magnitude selection in Jeffries et al. (2001), but not their two-color test (e.g. because of unrelated companions or weak cosmic rays). We have therefore checked where such stars fall in Figure 7*b*, and have found only 3 stars in the "acceptable" cluster region, for $1.0 \leq V - I \leq 1.5$. These are indeed good candidate cluster members. Their number is however so small that our conclusions remain unaffected.

5.5. X-Ray and Rotation

On the basis of the newly available rotational data (Terndrup et al. 2002), we have made a plot of L_X versus $v \sin i$, as shown in Figure 8. Unfortunately, $v \sin i$ is available for only 33 X-ray detected stars in our sample (2 F stars, 26 G stars, and 5 K stars), plus 18 undetected stars (1 A star, 5 F stars, 11 G stars, and 1 K star). Although there is not a tight correlation in these NGC 2516 data, the cloud of points for NGC 2516 follows rather well the relation $\log L_X = 27 + 2\log(v \sin i)$, found by Pallavicini et al. (1981) for late-type coronal sources (also plotted in Figure 8). The four upper limits at $\log v \sin i > 1.5$, clearly lower than the Pallavicini et al. relation, are all F stars. Here, we have split the observed L_X among components of equal-mass binary pairs (crosses in Figure 8), that gives a better agreement with the Pallavicini relation, albeit with a factor ~ 3 scatter (as said in section 5.3, some apparently single stars may actually be doubles as well). Therefore, it appears that NGC 2516 is not characterized by a peculiar dynamo mechanism acting in its stars, although this needs to be confirmed by more rotational data. Therefore, any dissimilarity with the Pleiades should be traced back to a dissimilarity in the rotational period distributions of the two clusters. Such a difference has been indeed found and discussed by Terndrup et al. (2002), who consider it in agreement with the known age difference between these clusters.

6. Conclusions

We have performed a comprehensive analysis of the Chandra imaging observations of the young cluster NGC 2516, studying both individual datasets and their combination, to achieve the highest sensitivity. Near cluster center, we detect cluster members with fluxes down to $\log f_X = -14.56$ (ergs/sec/cm^{-2}), or $\log L_X = 28.69$ (ergs/sec). Minimum detectable fluxes in the deepest individual datasets are about a factor 1.25-1.7 higher. The limiting X-ray luminosities reached by previous studies were $\log L_X \sim 29.0$ (ergs/sec) (Jeffries et al. 1997), $\log L_X \sim 29.3$ (ergs/sec) (Micela et al. 2000), $\log L_X \sim 28.65$ (ergs/sec) (Harnden et al. 2001 and Sciortino et al. 2001). We detect 284 unique X-ray sources, of which 155 identified with candidate cluster members from optical photometry. Thanks to the narrow Chandra PSF there is no ambiguity in the optical identifications, except for a handful of cases.

The detection rate as a function of spectral type is lowest for A and M stars (the latter being however contaminated by non-members), and is maximum for F stars, but never reaches 50%. We have attempted to evaluate the contamination for the different stellar types, and have built contamination-corrected X-ray luminosity functions, that differ significantly from the uncorrected distributions for G and later-type stars.

B stars show a large variety of X-ray luminosities, from strong emission to non-detection with low upper limits. The X-ray emission of the brightest B stars is not compatible with emission from lower-mass companions. The X-ray emission found (occasionally) in A stars is instead compatible with this hypothesis, but it remains unexplained why among these stars we detect nearly all chemically peculiar stars, and very few normal A stars.

The K stars X-ray luminosity function, corrected for contaminations, is significantly lower than the corresponding one in the Pleiades. This may be due in part to the (observed) reduced rotation rates of NGC 2516 stars with respect to their Pleiades analogues, but it is unclear if this may account for the whole difference. Less significant differences (around 2-σ level) are found instead in the luminosity functions of G and M stars (slightly lower in NGC 2516 than in the Pleiades), and of F stars (slightly higher in NGC 2516 than in the Pleiades).

At least some among binary F and G stars in NGC 2516 are overactive with respect to single F and G stars. Instead, NGC 2516 K binaries seem slightly underactive compared to single K stars, but the significance of this result depends much on the selection of an uncontaminated member/binary sample.

The reduced X-ray activity level in the G and K stars in NGC 2516 was already observed using previous X-ray data, and it was attibuted to a presumed low metallicity of NGC 2516 stars. Recent studies have derived instead solar-like abundances for NGC 2516, and have left only the small age difference between this cluster and the Pleiades as the most plausible reason to explain their different X-ray emission. Also the dependence of X-ray emission on stellar rotation for NGC 2516 stars appears quite normal.

The sample of NGC 2516 stars for which detailed optical spectra are now available, however, is rather small, and limited to early-G at the latest, while K stars show the largest discrepancy of X-ray activity levels with the Pleiades. As remarked by Terndrup et al. (2002), spectra of these later-type stars, on which a more complete study may be based, will be obtainable using telescopes of the 8-10 m class, that are just now becoming available.

FD, EF, GM, and SS acknowledge support from the italian ASI and MIUR. SJW acknowledges support from the Chandra X-Ray Center under NASA contract NAS8-39073. We all are grateful to the Chandra staff for the achievements made possible by this mission.

REFERENCES

Borra, E. F., Landstreet, J. D., & Mestel, L. 1982, ARA&A, 20, 191

Dachs, J. 1970, A&A, 5, 312

Dachs, J., Hummel, W. 1996, A&A, 312, 818

Damiani, F., Maggio, A., Micela, G., & Sciortino, S. 1997a, ApJ, 483, 350

Damiani, F., Maggio, A., Micela, G., & Sciortino, S. 1997b, ApJ, 483, 370

Drake, S. A., Linsky, J. L., Schmitt, J. H. M. M., Rosso, C. 1994, ApJ, 420, 387

Feigelson, E. D., & Nelson, P. I. 1985, ApJ, 293, 192

Flaccomio, E., Damiani, F., Micela, G., Sciortino, S., Harnden, F. R., Murray, S. S., Wolk, S. J. 2002, ApJ, in press

Gagnè, M., Caillault, J.-P., & Stauffer, J. R. 1995, ApJ, 450, 217

Giacconi, R., et al. 2001, ApJ, 551, 624

Guillout, P., Sterzik, M. F., Schmitt, J. H. M. M., Motch, C., Neuhäuser, R. 1998, A&A, 337, 113

Harnden, F. R., Jr., et al. 2001, ApJ, 547, L141

Jeffries, R. D, Thurston, M. R., & Pye, J. P. 1997, MNRAS, 287, 350

Jeffries, R. D, Thurston, M. R., & Hambly, N. C. 2001, A&A, 375, 863

Mermilliod, J.-C. 1981, A&A, 97, 235

Mermilliod, J.-C., Turon, C., Robichon, N., Arenou, F., & Lebreton, Y. 1997, in Hipparcos Venice '97, ed. M. A. C. Perryman, & P. L. Bernacca, 643

Micela, G., Sciortino, S., Kashyap, V., Harnden, F. R., Jr., Rosner, R. 1996, ApJS, 102, 75

Micela, G., Sciortino, S., Harnden, F. R., Jr., et al. 1999, A&A, 341, 751

Micela, G., Sciortino, S., Jeffries, R. D., Thurston, M. R., Favata, F. 2000, A&A, 357, 909

Pallavicini, R., Golub, L., Rosner, R., Vaiana, G. S., Ayres, T., Linsky, J. L. 1981, ApJ, 248, 279

Pye, J. P., Hodgkin, S. T., Stern, R. A., Stauffer, J. R. 1994, MNRAS, 266, 798

Robichon, N., Arenou, F., Mermilliod, J.-C., Turon, C. 1999, A&A, 345, 471

Sciortino, S., et al. 2001, A&A, 365, L259

Snowden, M. S. 1975, PASP, 87, 721

Terndrup, D. M., Pinsonneault, M., Jeffries, R. D, Ford, A., Stauffer, J. R., Sills, A. 2002, astro-ph/0205300

Tozzi, P., et al. 2001, ApJ, 562, 42

Wolk, S. J., et al. 2002, ApJ, in preparation

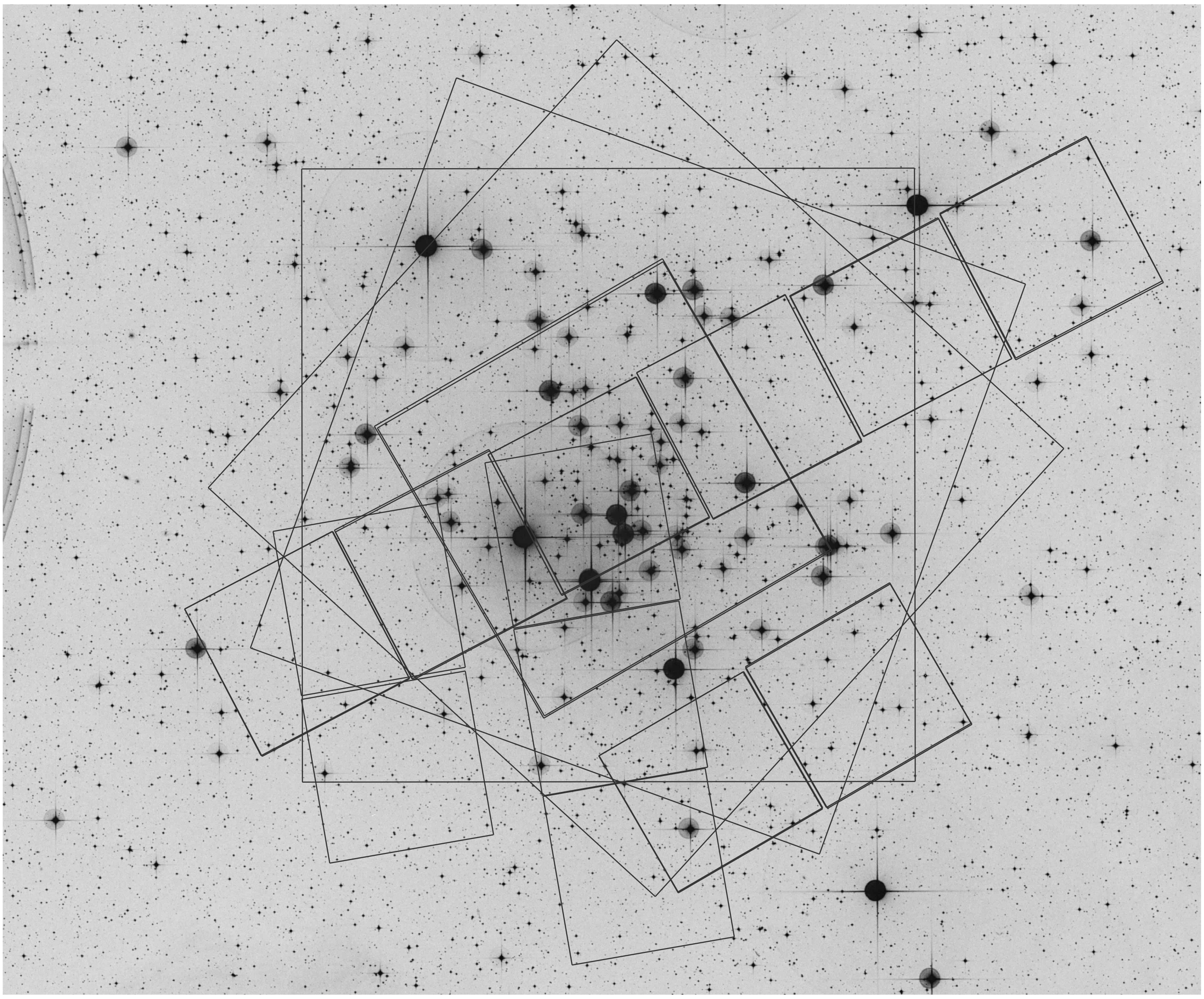

Fig. 1.— Optical DSS image of NGC 2516, with indicated fields of view of all Chandra pointings considered in this work. Large squares: HRC-I; intermediate squares: ACIS-I; small squares: single ACIS chips. North is up and East to the left.

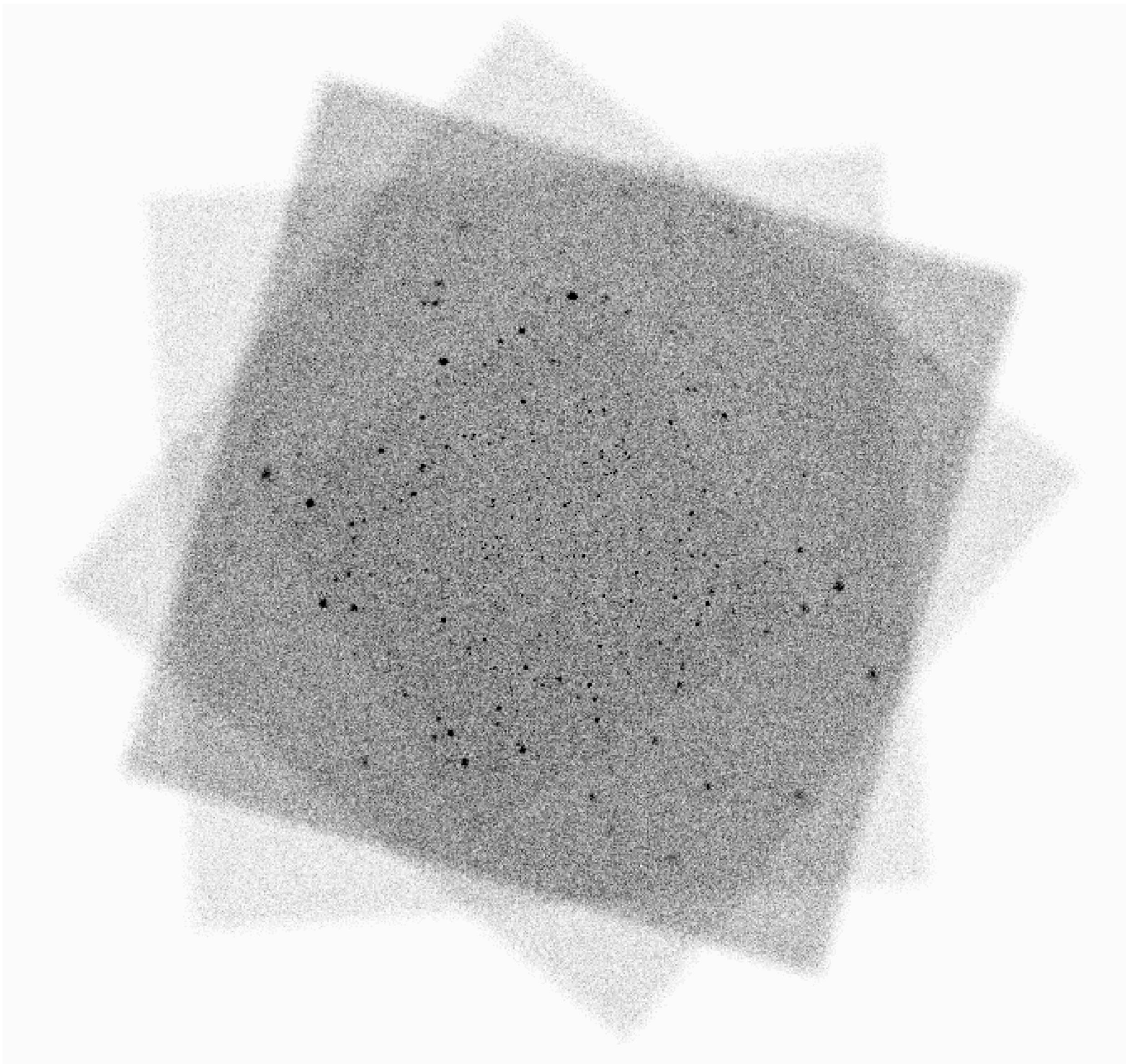

Fig. 2.— Combined Chandra X-ray image of NGC 2516, made using 3 HRC-I and 2 ACIS-I datasets. North is up and East to the left.

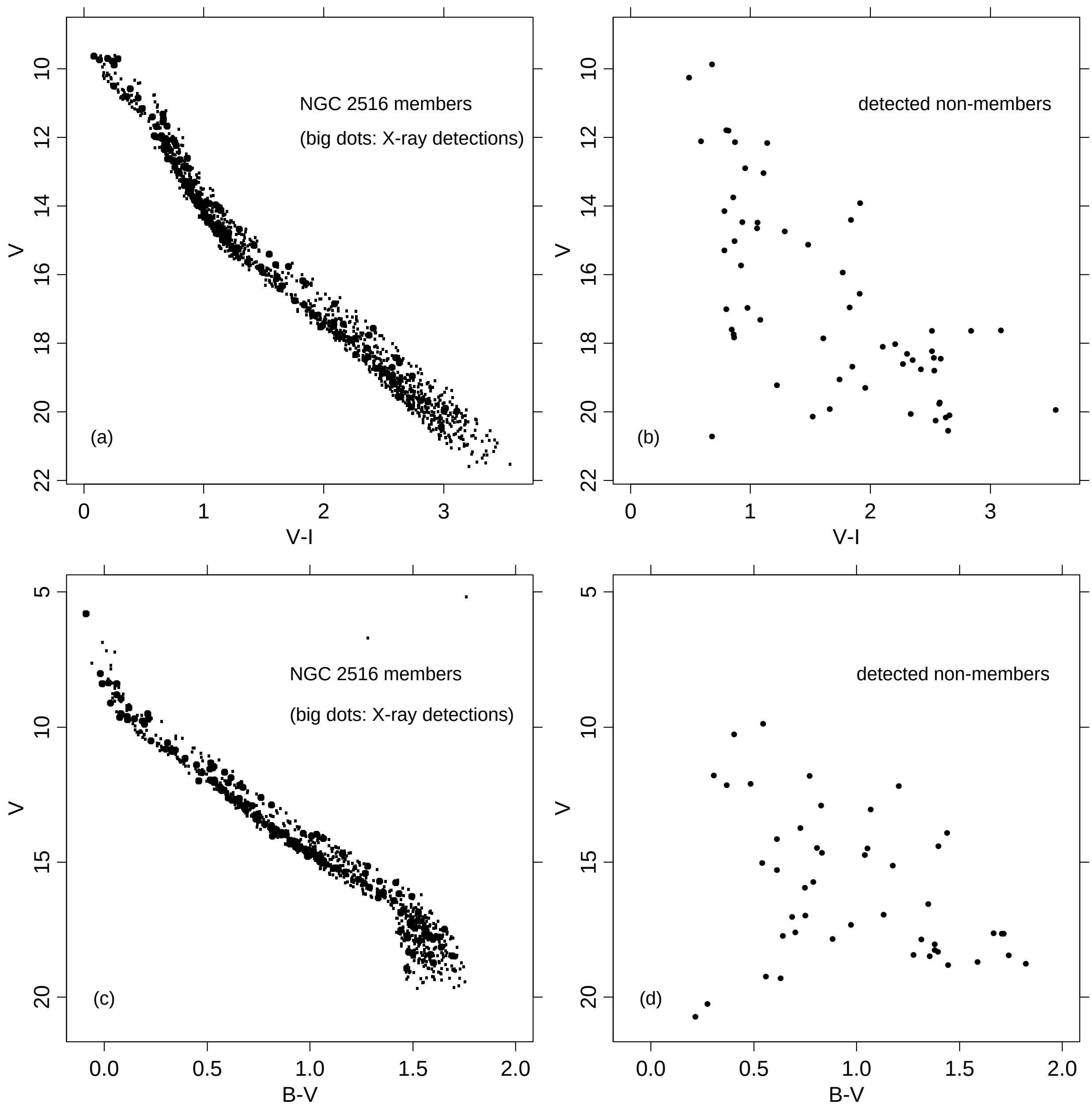

Fig. 3.— (*a*): $(V, V-I)$ Color-magnitude diagram for NGC 2516 members, with detected members marked as big dots. Since the $V-I$ color of the brightest stars is not available, they are missed in this plot. (*b*): $(V, V-I)$ Color-magnitude diagram for non-members detected as X-ray sources in our Chandra data. A few among them fall in the same region as NGC 2516 members, but have a $B-V$ color incompatible with membership. Faint, relatively blue objects may well be extragalactic. (*c*): $(V, B-V)$ Color-magnitude diagram for NGC 2516 members, with detected members marked as big dots. This diagram includes all brighter members. (*d*): $(V, B-V)$ Color-magnitude diagram for detected non-members.

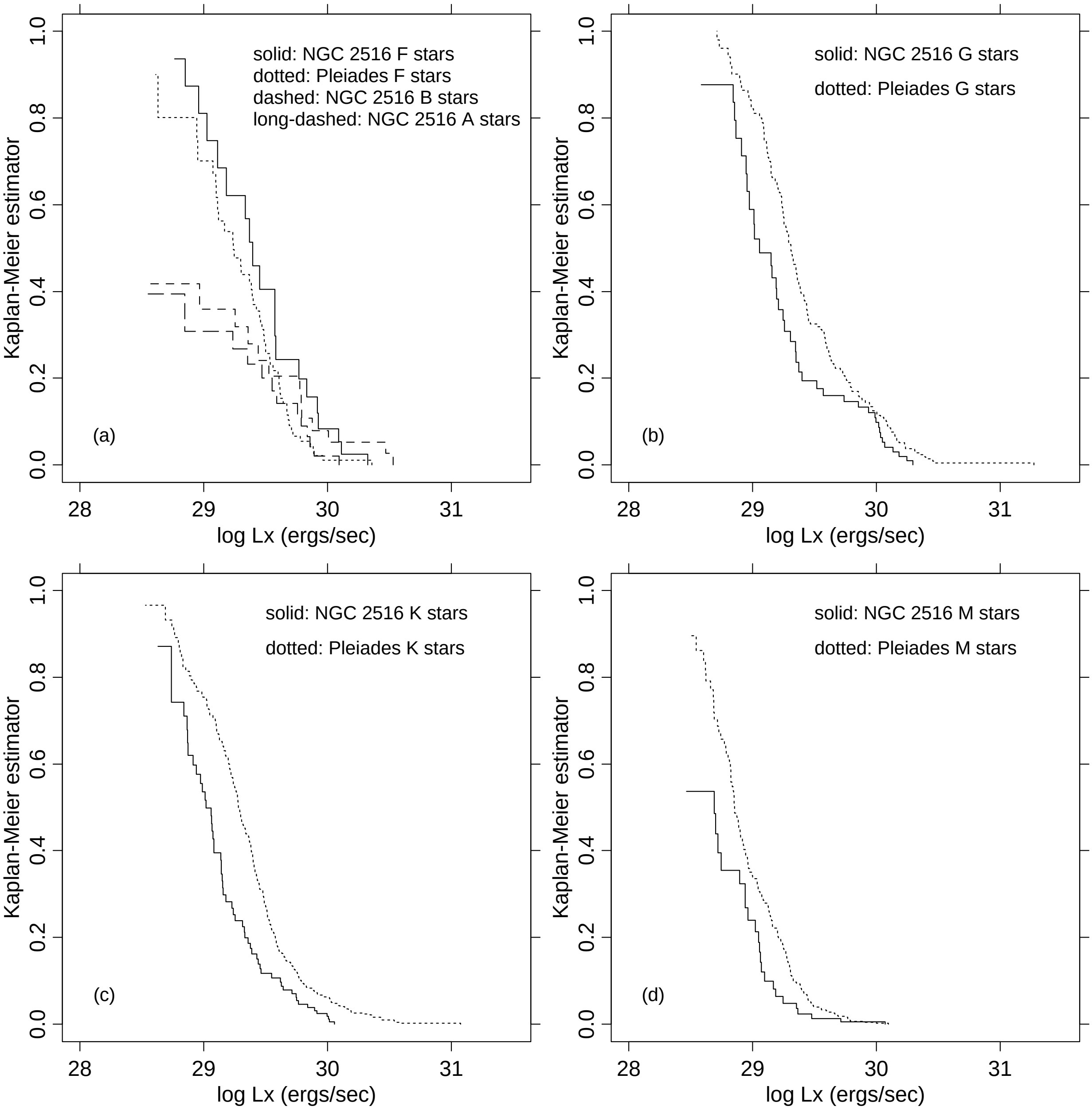

Fig. 4.— Maximum-likelihood X-ray luminosity functions for NGC 2516, separately for different spectral types (not corrected for contaminants), and comparison with analogous luminosity functions for the Pleiades (from Micela et al. 1999). (*a*): solid line: NGC 2516 F stars, dotted line: Pleiades F stars, dashed line: NGC 2516 B stars, long-dashed line: NGC 2516 A stars; (*b*): solid line: NGC 2516 G stars, dotted line: Pleiades G stars; (*c*): solid line: NGC 2516 K stars, dotted line: Pleiades K stars; (*d*): solid line: NGC 2516 M stars, dotted line: Pleiades M stars.

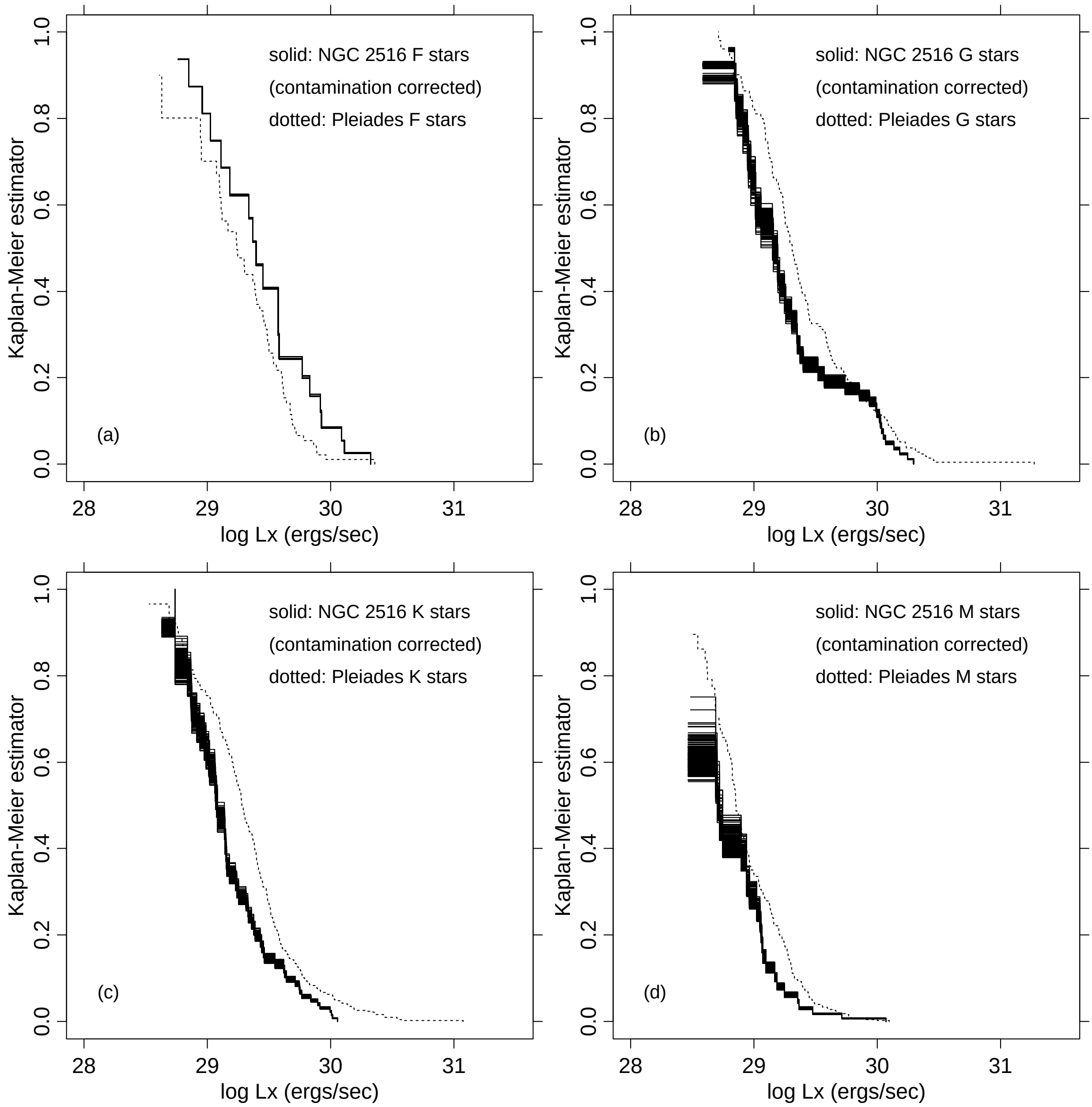

Fig. 5.— X-ray luminosity functions for NGC 2516 (solid lines), separately for different spectral types, corrected statistically for non-member contamination (see text). Each luminosity function was simulated 200 times. Also shown for comparison are the Pleiades luminosity functions (dotted). After correction, only the NGC 2516 K star luminosity function remains significantly different from its analogue in the Pleiades. (*a*): F stars; (*b*): G stars; (*c*): K stars; (*d*): M stars.

This preprint was prepared with the AAS LaTeX macros v5.0.

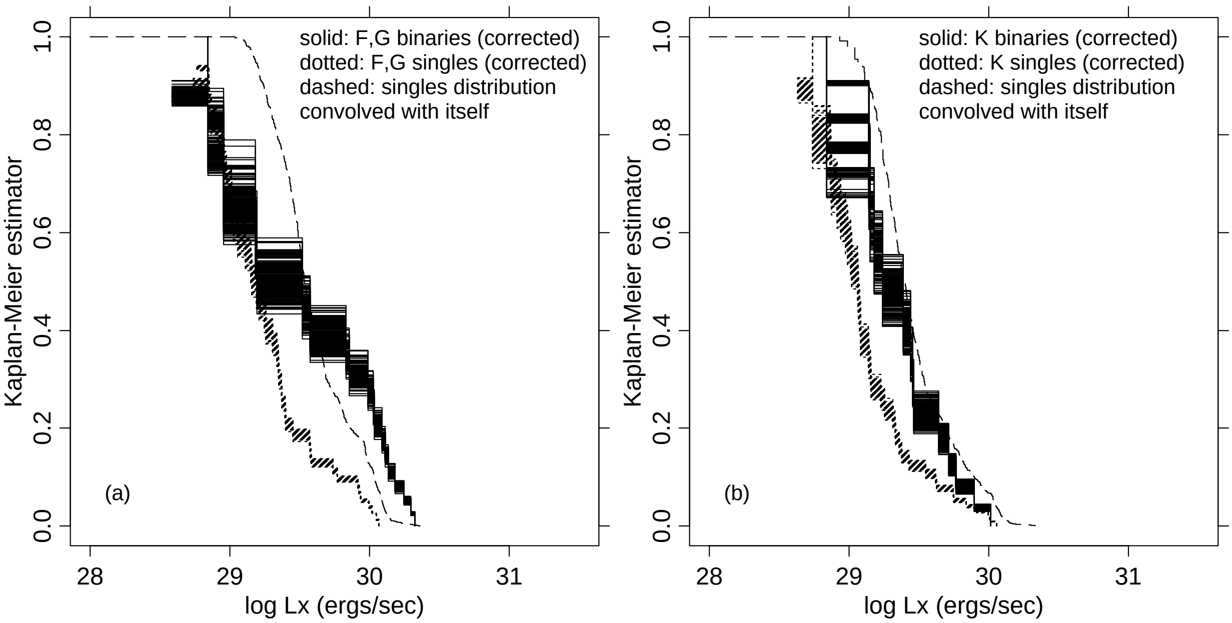

Fig. 6.— Comparison of (photometric) single- (dotted) and binary-stars (solid) X-ray luminosity functions (contamination-corrected), and the convolution of the single-star distribution with itself (dashed). (*a*): F and G stars; (*b*): K stars.

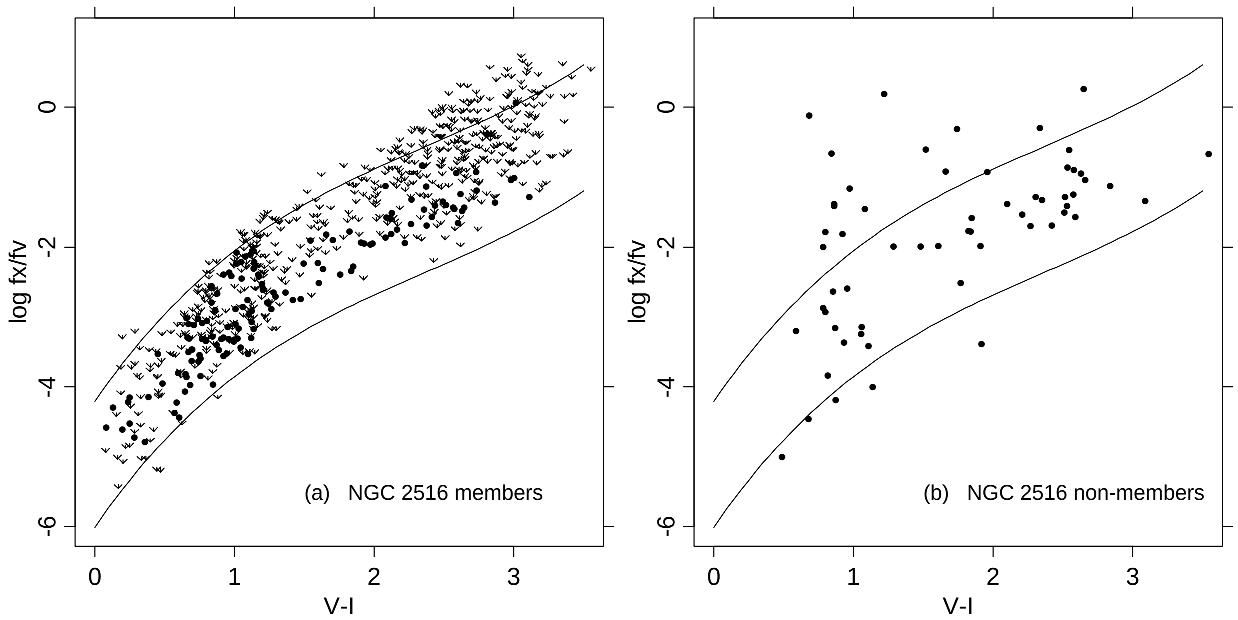

Fig. 7.— Plot of $\log f_X/f_V$ vs. $V-I$ color, for NGC 2516 members (a), and detected non-members (b). Many non-members fall in the same region as cluster members, and may be active young stars. Other objects have a much larger f_X/f_V for their $V-I$, and are probably non-coronal sources.

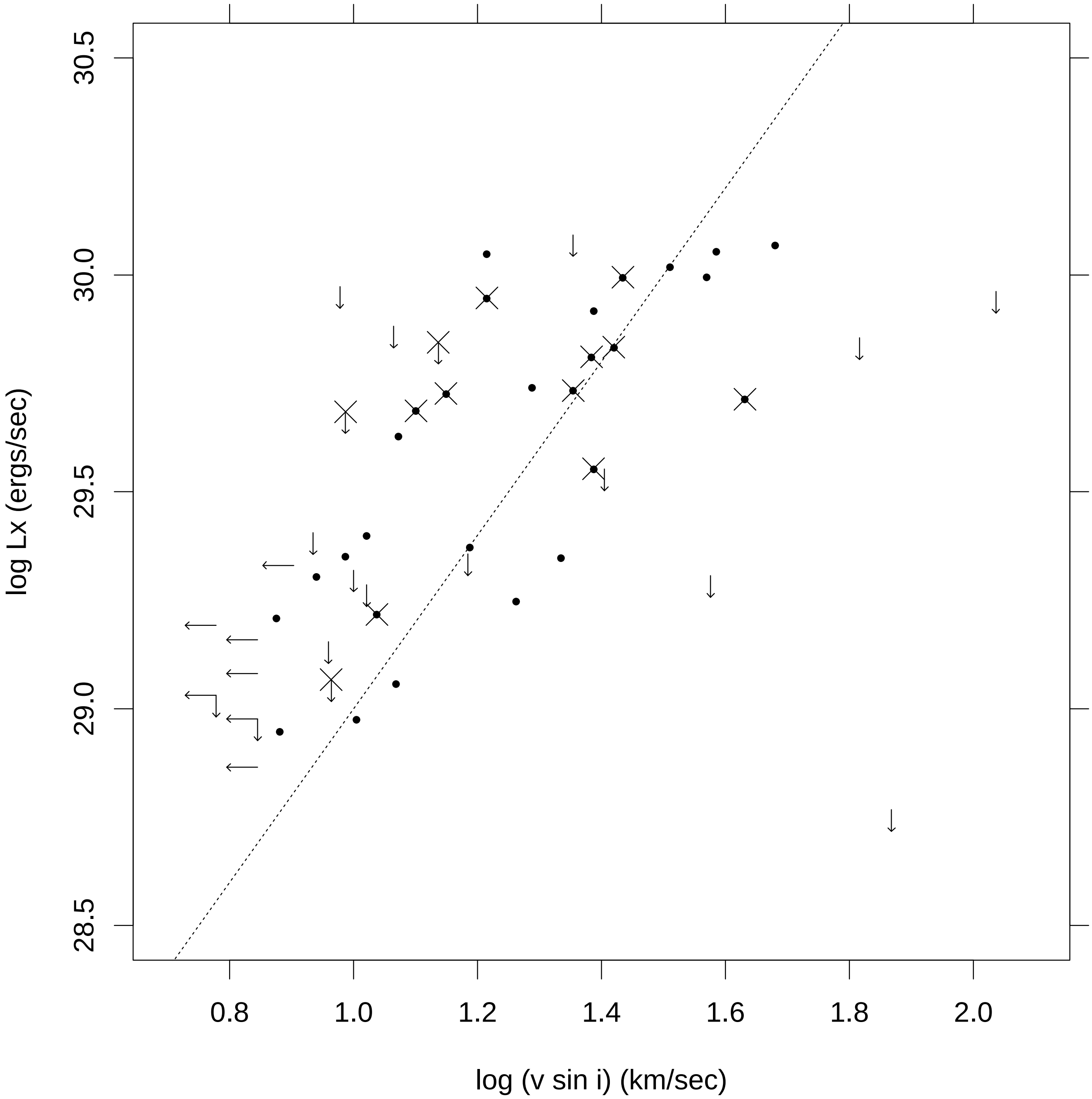

Fig. 8.— Plot of L_X vs. $v \sin i$ for NGC 2516 members. Binaries are indicated with crosses, and their X-ray luminosity was divided by two in this plot. Also indicated is the Pallavicini et al. (1981) relation (dotted line). Most points in this plot are G stars. The four discrepant upper limits at large $v \sin i$ are all F stars.